

# Merger Criteria of Multiple Massive Black Holes and the Impact on the Host Galaxy

A. Tanikawa<sup>1,2,3\*</sup> and M. Umemura<sup>1</sup>

<sup>1</sup>*Center for Computational Sciences, University of Tsukuba, 1-1-1, Ten-nodai, Tsukuba, Ibaraki 305-8577, Japan*

<sup>2</sup>*School of Computer Science and Engineering, University of Aizu, Tsuruga, Ikki-machi, Aizu-Wakamatsu, Fukushima 965-8580, Japan*

<sup>3</sup>*RIKEN Advanced Institute for Computational Science, 7-1-26, Minatojima-minami-machi, Chuo-ku, Kobe, Hyogo, 650-0047, Japan*

Accepted 1988 December 15. Received 1988 December 14; in original form 1988 October 11

## ABSTRACT

We perform  $N$ -body simulations on a multiple massive black hole (MBH) system in a host galaxy to derive the criteria for successive MBH merger. The calculations incorporate the dynamical friction by stars and general relativistic effects as pericentre shift and gravitational wave recoil. The orbits of MBHs are pursued down to ten Schwarzschild radii ( $\sim 1\text{AU}$ ). As a result, it is shown that about a half of MBHs merge during 1 Gyr in a galaxy with mass  $10^{11}M_{\odot}$  and stellar velocity dispersion  $240\text{ km s}^{-1}$ , even if the recoil velocity is two times as high as the stellar velocity dispersion. The dynamical friction allows a binary MBH to interact frequently with other MBHs, and then the decay of the binary orbits leads to the merger through gravitational wave radiation, as shown by Tanikawa & Umemura (2011). We derive the MBH merger criteria for the masses, sizes, and luminosities of host galaxies. It is found that the successive MBH mergers are expected in bright galaxies, depending on redshifts. Furthermore, we find that the central stellar density is reduced by the sling-shot mechanism and that high-velocity stars with  $\sim 1000\text{ km s}^{-1}$  are generated intermittently in extremely radial orbits.

**Key words:** black hole physics — galaxies: nuclei — methods: numerical

## 1 INTRODUCTION

Massive black holes (hereafter MBHs) with the mass of more than  $10^6$  solar mass ( $M_{\odot}$ ) have been found in the centres of galaxies. The mass of MBHs is correlated with the properties of the spheroidal components of their host galaxies, with respect to the mass (Kormendy & Richstone 1995; Magorrian et al. 1998; Marconi & Hunt 2003), the velocity dispersions (Ferrarese & Merritt 2000; Tremaine et al. 2002; Gültekin et al. 2009), and the number of globular clusters (Burkert & Tremaine 2010; Harris & Harris 2011). The origin of MBHs is an open issue of great significance.

In the last decade, quasars (QSOs) that possess  $\sim 10^9 M_{\odot}$  MBHs have been found at high redshifts of  $z \gtrsim 6$  (e.g., Fan et al. 2001), that is, at the cosmic age of  $\lesssim 1$  Gyr. Conservatively speaking, the seeds of the MBHs could be stellar mass black holes as massive star remnants. In particular, the remnants of first stars are one of plausible candidates, since first stars are likely to be as massive as a few hundred solar mass (Abel, Bryan & Norman 2000; Nakamura & Umemura 2001; Bromm, Coppi & Larson 2002; Yoshida et al. 2006),

several tens solar mass (Clark et al. 2011), or about  $50M_{\odot}$  (Hosokawa et al. 2011). However, in order for first star remnants to grow up to  $\sim 10^9 M_{\odot}$  in 1 Gyr, the Eddington ratio of mass accretion rate should be larger than unity (e.g., Umemura 2001; Greene 2012, and references therein). Super-Eddington accretion is one of possible solutions for the MBH growth (e.g. Abramowicz et al. 1988; Kawaguchi 2003; Ohsuga et al. 2005). On the other hand, the integration of the QSO luminosity function is concordant with the integrated mass function of MBHs in the local universe, as long as the Eddington ratios are between 0.1 and 1.7 (Soltan 1982; Yu & Tremaine 2002; Marconi et al. 2004). This implies that supermassive black holes acquire the bulk of mass through gas accretion in the late evolutionary stages and the mass accretion rates are not highly super-Eddington. Also, the gas accretion onto the seeds should be intermittent, and on average could be lower than the Eddington accretion rate (Milosavljevic, Couch & Bromm 2009a; Milosavljevic et al. 2009b). If the merger of multiple black holes precedes the growth via gas accretion, the merged MBH can be a seed of a supermassive black hole, and therefore the constraint for the BH growth can be weaker.

\* E-mail: ataru.tanikawa@riken.jp

In the cold dark matter cosmology, larger galaxies form

hierarchically through mergers of smaller galaxies. Hence, many MBHs are assembled in a larger galaxy, if smaller galaxies already possess MBHs. Furthermore, MBHs could be born in hyper-massive star clusters formed by galaxy collisions (Matsui et al. 2011). Thus, galaxy merger remnant can contain many MBHs, even if precursory galaxies have no MBHs.

Observationally, multiple active galactic nucleus (AGN) systems have been discovered recently. They include a triple AGN in the galaxy SDSS J1027+1749 at  $z = 0.066$  (Liu, Shen & Strauss 2011), three rapidly growing MBHs of  $10^6 - 10^7 M_\odot$  in a clumpy galaxy at  $z = 1.35$  (Schawinski et al. 2011), a firstly-discovered physical quasar triplet QQQ J1432-0106 within the projected separation of  $30 - 50 \text{ kpc}$  at  $z = 2.076$  (Djorgovski et al. 2007), and a second quasar triplet QQQ J1519+0627 within the projected separation of  $200 \text{ kpc}$ , which is likely to be harboured in a yet-to-be-formed massive system at  $z = 1.51$  (Farina et al. 2013). According to the hierarchical merger history, galaxies with many MBHs are likely to form at higher redshifts. Although the galaxy merger proceeds through the violent relaxation, the merger of MBHs has difficulty. As pointed out in Begelman, Blandford & Rees (1980), two MBHs in a galaxy are likely to form a binary, but unlikely to merge directly due to the so-called loss cone depletion (the depletion of stars on orbits that intersect the binary MBH). A binary MBH cannot reach sub-parsec separation due to the loss cone depletion, which is called the final parsec problem (e.g. Merritt & Poon 2004). A possible way to evade the loss cone depletion is the nonaxisymmetric potential of the host galaxy (Merritt & Poon 2004; Berczik et al. 2006; Khan, Just & Merritt 2011; Khan et al. 2012), which is the natural consequence of the galaxy merger. A binary MBHs can merge in the nonaxisymmetric potential in  $10 \text{ Gyr}$  or  $0.3 \text{ Gyr}$ , when the galaxy contains stars with  $10^9 M_\odot$  or  $10^{11} M_\odot$ , respectively (Khan, Just & Merritt 2011). However, since this timescale is comparable to or longer than the galactic dynamical timescale, other galaxies harbouring MBHs can intrude before two MBHs merge. This is likely to occur at higher redshifts of  $z \gtrsim 6$ , at which the universe age is less than  $1 \text{ Gyr}$ . If there are more than two MBHs in a galaxy, the dynamical relaxation of MBHs is significantly controlled by the gravity of MBHs themselves, especially by three-body interaction. When a third MBH intrudes into a binary MBH, one of the three MBHs carries away angular momentum from the rest two MBHs, reducing the binary separation, and eventually the binary merges (e.g. Iwasawa, Funato & Makino 2006).

So far, galaxy structures have not been investigated when the galaxies contain more than three MBHs, although they have been investigated in the cases of two MBHs (e.g. Khan, Just & Merritt 2011; Khan et al. 2012) and three MBHs (e.g. Iwasawa, Funato & Makino 2008). Tanikawa & Umemura (2011) (hereafter, paper I) scrutinised a system of multiple MBHs in a galaxy by high-resolution  $N$ -body simulations, and found that multiple MBHs produce one dominant MBH through successive mergers. Binary MBHs lose their angular momentum owing to sling-shot mechanism, which induces the decay of the binary orbits through gravitational wave (GW) radiation. In paper I, we investigated one model of a galaxy containing multiple MBHs. In this paper, we explore the

evolution of multiple MBHs in galaxies with different 3-dimensional stellar velocity dispersions to derive the criteria of the MBH merger. We also consider the effect of the recoil by anisotropic GW radiation at the MBH merger. Since the recoil velocity typically reaches several hundred  $\text{km s}^{-1}$  (Kesden, Sperhake & Berti 2010), it could suppress the MBH growth. Furthermore, we investigate the impact by the MBH merger on the galaxy structure.

The paper is organised as follows. In section 2, we describe the simulation model. In section 3, we show numerical results. In section 4, the results are translated to derive the criteria for MBH merger, which are applied for high and low redshift galaxies. In section 5, the back-reaction to a host galaxy is discussed with respect to the galactic structure and the production of high velocity stars. In section 6, we summarise this paper.

## 2 MODEL

### 2.1 Initial conditions

We consider a model galaxy that initially contains ten MBHs of equal mass. The effect by the inequality of MBH mass has been explored by several authors (e.g. Iwasawa et al. 2011; Khan et al. 2012). In the present simulation, an unequal mass binary forms as a consequence of the MBH merger. The case in which unequal mass MBHs are set up initially will be investigated elsewhere. Stars in a galaxy are treated as superparticles. The number of stars is  $N = 512k$  ( $1k = 1024$ ). The stars are initially distributed according to the Hernquist's profile, where the mass density distribution is given by

$$\rho(r) = \frac{M_g}{6\pi r_g^3} \frac{1}{(r/r_g)[(r/r_g) + 1/3]^3}, \quad (1)$$

where  $M_g$  and  $r_g$  are respectively the total mass and virial radius of the host galaxy. Here,  $r_g$  is given by

$$r_g = \frac{GM_g}{2v_g^2}, \quad (2)$$

with the gravitational constant  $G$  and the 3-dimensional stellar velocity dispersion  $v_g$ .

The mass of MBH is set to be  $0.01 \%$  of the galaxy mass. So, the total mass of ten MBHs is  $0.1 \%$  of the galaxy mass. We realise the distribution of MBHs as follows. The distribution function is supposed to be the same as that of stars within one-third of  $r_g$  (see Paper I for the dependence on the spread). First, we generate positions and velocities for stars according to the above distributions. Next, we convert ten stars into ten MBHs; we choose randomly ten stars from the stars within one-third of  $r_g$ .

The 3-dimensional velocity dispersion,  $v_g$ , is one of key parameters in the present simulations. Note that the velocity dispersion in this paper is 3-dimensional unless otherwise noted. We consider several galaxy models with different velocity dispersions. The assumed models are shown in Table 1. In models A, the velocity dispersion is  $v_g = 350 \text{ km s}^{-1}$ , where  $A_{0,1}$ ,  $A_{0,2}$ , and  $A_{0,3}$  are based on different sets of random numbers. In models B, C, and D,  $v_g = 240$ ,  $180$ , and  $120 \text{ km s}^{-1}$ , respectively. In models  $A_1$ ,  $B_1$ , and  $C_1$ , the recoil velocity,  $v_{\text{recoil}}$ , is added after the MBH merger.

Also, for the comparison to models with ten MBHs, we perform simulations for galaxies without MBHs (model BH0) and with two MBHs (model BH2).

In the present simulations, we adopt the standard  $N$ -body units, where  $G = M_g = r_g = 1$ . Then,  $v_g = 1/\sqrt{2}$  from Equation (2). The speed of light,  $c$ , is required to be redefined in the present units, since we include Post-Newtonian (PN) corrections (described later). The speed of light changes as  $c = 6.06 \times 10^2$ ,  $8.84 \times 10^2$ ,  $1.18 \times 10^3$ , or  $1.77 \times 10^3$  for models A, B, C, or D, respectively.

After we determine the velocity dispersion,  $v_g$ , we still have one free parameter, although  $M_g/r_g$  is fixed for each  $v_g$  (see Equation (2)). Setting either of the galaxy mass  $M_g$  or the galactic virial radius  $r_g$ , we can transform the code units to physical units. When we set  $M_g$ , we express  $r_g$  and the dynamical time at  $r_g$  as follows:

$$r_g \simeq 1.76 \left( \frac{M_g}{10^{11} M_\odot} \right) \left( \frac{v_g}{350 \text{ km s}^{-1}} \right)^{-2} [\text{kpc}], \quad (3)$$

and

$$t_{\text{dy},g} = \frac{r_g}{\sqrt{2}v_g} \simeq 3.47 \left( \frac{M_g}{10^{11} M_\odot} \right) \left( \frac{v_g}{350 \text{ km s}^{-1}} \right)^{-3} [\text{Myr}]. \quad (4)$$

We show  $M_g$  when  $r_g = 1$  kpc in the rightmost column of Table 1, which is derived from Equation (3). The average mass density inside  $r_g$  is given as

$$\rho_g = \frac{27M_g}{64\pi r_g^3} \simeq 2.48 \left( \frac{M_g}{10^{11} M_\odot} \right)^{-2} \left( \frac{v_g}{350 \text{ km s}^{-1}} \right)^6 [M_\odot \text{ pc}^{-3}]. \quad (5)$$

## 2.2 Equation of motion

The equations of motion for field stars and MBHs are respectively given by

$$\frac{d^2 \mathbf{r}_{f,i}}{dt^2} = \sum_{j \neq i}^{N_f} \mathbf{a}_{ff,ij} + \sum_j^{N_B} \mathbf{a}_{fB,ij}, \quad (6)$$

$$\frac{d^2 \mathbf{r}_{B,i}}{dt^2} = \sum_j^{N_f} \mathbf{a}_{Bf,ij} + \sum_{j \neq i}^{N_B} \mathbf{a}_{BB,ij}, \quad (7)$$

where  $\mathbf{r}_{f,i}$  and  $\mathbf{r}_{B,i}$  are the position vectors of  $i$ -th field star and  $i$ -th MBH,  $N_f$  and  $N_B$  are the numbers of field stars and MBHs,  $\mathbf{a}_{ff,ij}$  and  $\mathbf{a}_{fB,ij}$  are the accelerations by  $j$ -th field star and  $j$ -th MBH on  $i$ -th field star, and  $\mathbf{a}_{Bf,ij}$  and  $\mathbf{a}_{BB,ij}$  are the accelerations by  $j$ -th field star and  $j$ -th MBH on  $i$ -th MBH, respectively. Excepting the MBH-MBH interaction, the accelerations are given by Newtonian gravity:

$$\mathbf{a}_{ff,ij} = -Gm_{f,j} \frac{\mathbf{r}_{f,i} - \mathbf{r}_{f,j}}{(|\mathbf{r}_{f,i} - \mathbf{r}_{f,j}|^2 + \epsilon^2)^{3/2}} \quad (8)$$

$$\mathbf{a}_{fB,ij} = -Gm_{B,j} \frac{\mathbf{r}_{f,i} - \mathbf{r}_{B,j}}{|\mathbf{r}_{f,i} - \mathbf{r}_{B,j}|^3} \quad (9)$$

$$\mathbf{a}_{Bf,ij} = -Gm_{f,j} \frac{\mathbf{r}_{B,i} - \mathbf{r}_{f,j}}{|\mathbf{r}_{B,i} - \mathbf{r}_{f,j}|^3}, \quad (10)$$

where  $m_{f,j}$  and  $m_{B,j}$  are respectively the masses of  $j$ -th field star and  $j$ -th MBH, and the softening parameter ( $\epsilon = 10^{-3}$ ) is introduced only in star-star interactions.

The acceleration between two MBHs is composed of the Newtonian gravity and PN corrections, such as

$$\mathbf{a}_{BB,ij} = -Gm_{B,j} \frac{\mathbf{r}_{B,i} - \mathbf{r}_{B,j}}{|\mathbf{r}_{B,i} - \mathbf{r}_{B,j}|^3} + \mathbf{a}_{\text{PN},ij}. \quad (11)$$

We explain the second term below.

## 2.3 Relativistic effects

We incorporate the general relativistic effects on the orbits of MBHs, that is, the pericentre shift, GW radiation, and GW recoil. We model the pericentre shift and GW radiation by including the second term ( $\mathbf{a}_{\text{PN},ij}$ ) in Equation (11) up to 2.5PN term. The pericentre shift corresponds to 1PN and 2PN terms, and the GW radiation does to 2.5PN term (Damour & Dervelle 1981; Soffel 1989; Kupa, Amaro-Seoane & Spurzem 2006). We employ Equations (1), (2), (3), and (4) in Kupa, Amaro-Seoane & Spurzem (2006) for the general relativistic corrections.

Also, we model the GW recoil as follows. At the moment when two MBHs merge, we add recoil velocities to the merged MBHs. Their absolute values are fixed in each simulation. Their direction is determined by the Monte-Carlo method, assuming the isotropic probability. In practice, the absolute values of recoil velocities widely range from several ten  $\text{km s}^{-1}$  to several thousand  $\text{km s}^{-1}$ , and their directions are determined by the mass ratio and spins of two MBHs (Campanelli et al. 2007; Lousto et al. 2010). However, if their spins are aligned before their merger due to relativistic spin precession (Kesden, Sperhake & Berti 2010), then the recoil velocity decreases to a few  $100 \text{ km s}^{-1}$ . The recoil velocity  $v_{\text{recoil}}$  in each simulation is summarised in Table 1. We set the recoil velocity to be equal to or more than  $200 \text{ km s}^{-1}$ , excepting models without the recoil.

## 2.4 Merger condition

We assume that two MBHs merge, when the separation between two MBHs is less than ten times the sum of their Schwarzschild radii:

$$|\mathbf{r}_{B,i} - \mathbf{r}_{B,j}| < 10(r_{\text{sch},i} + r_{\text{sch},j}), \quad (12)$$

where  $r_{\text{sch},i}$  is the Schwarzschild radius of  $i$ -th MBH that is  $2Gm_{B,i}/c^2$  for the MBH mass  $m_{B,i}$  with the speed of light  $c$ .

## 2.5 Numerical scheme

Since our numerical scheme is the same as that in paper I, we describe its outline here. We adopt a fourth-order Hermite scheme with individual timestep scheme (Makino & Aarseth 1992) for time integration method for an MBH and a star.

For compact binary MBHs, we transform their motions to their relative motion and the centre-of-mass motion. The relative motions are integrated in the same way as single MBHs and stars. In calculating tidal forces on the binary MBHs, we consider the other MBHs and nearby stars as perturbers, and ignore perturbation by the rest of stars. A perturber of a binary MBH is defined as a particle whose distance from the binary MBH is smaller than 200 times

of the semi-major axis of the binary MBH. For the centre-of-mass motion, we adopt Hermite Ahmad-Cohen scheme (Makino & Aarseth 1992) for time integration.

We perform  $N$ -body simulations with the FIRST simulator (Umemura et al. 2008) at University of Tsukuba. We use 64 nodes of the FIRST simulator. Each node is equipped with one Blade-GRAPE, which is one of GRAPEs: a special purposed accelerator for a collisional  $N$ -body system (Sugimoto et al. 1990; Makino et al. 2003; Fukushima, Makino & Kawai 2005). We compute gravitational forces exerting on a given particle in parallel, which is the so-called  $j$ -parallel algorithm.

### 3 NUMERICAL RESULTS

#### 3.1 Model dependence

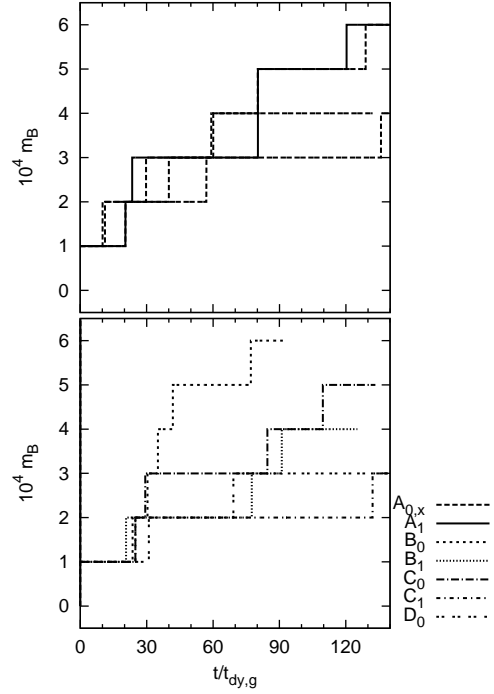
We have calculated a system of ten MBHs in one galaxy during about  $140 t_{\text{dy,g}}$ , which corresponds to about 1 Gyr in physical units if we adopt  $M_g = 10^{11} M_\odot$  and  $v_g = 240 \text{ km s}^{-1}$ . The models and results are summarised in Table 1. The first and second columns indicate the model name and the number of MBHs, respectively. Models  $A_{0,1}$ ,  $A_{0,2}$ , and  $A_{0,3}$  corresponds to models  $A_1$ ,  $A_2$ , and  $A_3$  in Paper I, respectively. The third column is the stellar velocity dispersion. In the fourth and fifth columns, we show the assumed GW recoil velocity and the ratio of the recoil velocity to the velocity dispersion, respectively. As numerical results, we show the mass of the heaviest MBH ( $m_{\text{B,p}}$ ) and the second heaviest MBH ( $m_{\text{B,s}}$ ) in the sixth and seventh columns, respectively. Their mass is scaled by the initial MBH mass. If the heaviest or second heaviest MBHs are ejected from the galaxy centre, we attach “(e)” beside their mass. The number of MBHs ejected from the galaxy centre ( $N_{\text{B,ej}}$ ) is shown in the eighth column. We define the ejected MBHs to be far by more than  $r_g$  from the galaxy centre. The galaxy centre is obtained from the density centre of stars, which is calculated in the same way as Casertano & Hut (1985).

Fig. 1 shows the time evolution of the mass of the heaviest MBH in each model. In each of model A, B, and  $C_0$ , one dominant MBH grows in a galaxy. They are formed through mergers of 4 – 6 MBHs. In some of these models, other MBHs become heavier than the initial ones. However, they are ejected from the galaxy through sling-shot mechanism by three MBH interaction. They are not ejected by the GW recoil, since the GW recoil is set to be at most  $2v_g$ , while the escape velocity of our galaxy models is about  $4v_g$  (described below in detail). In these models, about a half of MBHs successively merge in  $140 t_{\text{dy,g}}$ .

On the other hand, in models  $C_1$  and  $D_0$ , only three MBHs merge in  $140 t_{\text{dy,g}}$ . A heavier MBH might form, if we follow the evolution of the MBHs beyond  $140 t_{\text{dy,g}}$ . However, we do not follow their evolution, since artificial two-body relaxation may affect the merger for the present number of particles.

#### 3.2 Merger dynamics

Here, we see the merger process in detail, using the result of model  $A_1$ , which includes the GW recoil. The merger process is similar to that in the models without the GW recoil, i.e.,



**Figure 1.** Time evolution of the mass of the heaviest MBH in each model. Models  $A_{0,1}$ ,  $A_{0,2}$ , and  $A_{0,3}$  are brought together as “ $A_{0,x}$ ”. Models A are shown in the top panel, and the other in the bottom panel.

models  $A_{0,1}$ ,  $A_{0,2}$ , and  $A_{0,3}$ , in which the merger process is shown in Paper I. As seen in the top panel of Fig. 2, one MBH grows by the merger, and other MBHs do not grow by the terminal time of our simulation. Two MBHs temporarily merge at  $t_{\text{dy,g}} = 54$ . However, the merged MBH is swallowed by the heaviest MBH at  $t_{\text{dy,g}} = 80$ .

The result that only one MBH predominantly grows comes from the following three facts. Two MBHs merge only via a phase of a binary MBH (fact 1). The binary MBH tends to contain the heaviest MBH (fact 2). Furthermore, the binary MBH is unique in the galaxy at any time (fact 3). Fact 1 can be verified in the second top panel of Fig. 2. Binary MBHs have semi-major axes of  $10^{-5} r_g - 10^{-4} r_g$  for a long time until they merge. Fact 2 can be seen in the second bottom panel. The heaviest MBH is contained in a binary MBH through most of time (except during  $t_{\text{dy,g}} = 46 - 54$ ). This is because a binary MBH often experiences three MBH interactions, through which a heavier MBH is more easily retained in the binary MBH. Fact 3 can be confirmed in the bottom panel. For most of time, the number of binary MBHs in the galaxy is one or zero.

For the mergers of MBHs, the dynamical friction plays a key role. (see also Fig. 2 in Paper I). The dynamical friction by field stars allows MBHs to gather near the galaxy centre. Thus, two MBHs can compose a binary MBH, and subsequently another MBH can intrude the binary MBH. Then, the single MBHs interact with the binary MBH repeatedly and consequently the semi-major axis and eccentricity of the binary MBH are changed owing to the angular momentum loss. Such repeated interactions occur before most of mergers. However, the crucial impact is brought by one strong



**Table 1.** MBH mass and the number of ejected MBHs after  $140t_{\text{dy,g}}$ . The units of  $m_{\text{B,p}}$  and  $m_{\text{B,s}}$  are initial MBH mass.

Model	$N_B$	$v_g/\text{km s}^{-1}$	$v_{\text{recoil}}/\text{km s}^{-1}$	$v_{\text{recoil}}/v_g$	$m_{\text{B,p}}$	$m_{\text{B,s}}$	$N_{\text{B,ej}}$	$M_g/(10^{10}M_\odot)$ [ $r_g = 1\text{kpc}$ ]
A <sub>0,1</sub>	10	350	0	0	4	3(e)	2	5.7
A <sub>0,2</sub>	10	350	0	0	4	1	3	5.7
A <sub>0,3</sub>	10	350	0	0	6	1	1	5.7
A <sub>1</sub>	10	350	500	1.4	6	1	1	5.7
B <sub>0</sub>	10	240	0	0	6	1	1	2.7
B <sub>1</sub>	10	240	500	2.1	4	2(e)	2	2.7
C <sub>0</sub>	10	180	0	0	5	1	1	1.5
C <sub>1</sub>	10	180	200	1.1	3	2	1	1.5
D <sub>0</sub>	10	120	0	0	3	1	2	0.67
BH0	0	240	–	–	–	–	–	2.7
BH2	2	240	–	–	–	–	–	2.7

interaction, and thereby the distance of the binary MBH at the pericentre ( $r_p$ ) shrinks significantly, so that the GW radiation works effectively to lose the energy, eventually causing the merger of the binary.

Such merger process is not affected by the GW recoil, if the recoil velocity is of the order of the stellar velocity dispersion,  $v_g$ . A merged MBH is retained in the inner region of the galaxy, in which the stellar density is high. In this region, the dynamical friction effectively loses angular momenta of the merged MBH. Hence, the merged MBH falls again toward the galactic centre, and form a binary MBH with another single MBH. The binary MBH can interact again a third MBH.

Also, we have found that the secular angular momentum loss of a binary MBH through the Kozai mechanism (Kozai 1962) is not effective. The Kozai mechanism can work through eccentricity oscillation, if the semi-major axis ratio is small (Blaes, Lee & Socrates 2002; Berentzen et al. 2009). But, in our simulations, the semi-major axis ratio is too large to allow eccentricity oscillation. Instead, the relativistic pericentre shift (1PN and 2PN) is dominant. In fact, if we do not include the 1PN and 2PN terms, the Kozai mechanism works for a binary to merge. The suppression of the Kozai mechanism is also demonstrated in the case of stellar-sized black holes (Miller & Hamilton 2002) and in the planetary orbits (Fabrycky & Tremaine 2007).

## 4 CRITERIA FOR SUCCESSIVE MERGERS

### 4.1 Constraints for galaxy mass and size

From the above numerical results, we conclude that the lower limit of stellar velocity dispersion is  $v_g \sim 180 \text{ km s}^{-1}$ , when the GW recoil is  $200 \text{ km s}^{-1}$ . Regardless of whether the GW recoil is exerted or not, one dominant MBH grows in model B<sub>0</sub> and B<sub>1</sub>, in both of which the stellar velocity dispersion is more than  $240 \text{ km s}^{-1}$ . On the other hand, the growth of one dominant MBH depends on the GW recoil in models C in which galaxies have the stellar velocity dispersion of  $180 \text{ km s}^{-1}$ . The dependence of the MBH growth on the stellar velocity dispersion can be understood as follows. Using Equation (2), we express the ratio of a Schwarzschild

radius of an MBH to the virial radius of the galaxy as

$$\frac{r_{\text{sch},i}}{r_g} = 4 \left( \frac{m_{\text{B},i}}{M_g} \right) \left( \frac{v_g}{c} \right)^2. \quad (13)$$

This means that the MBH horizon size is smaller compared to the galaxy size if the stellar velocity dispersion is smaller. Therefore, a larger amount of angular momenta should be extracted for a binary MBH to merger, so that the resultant largest MBH becomes less massive.

Here, we estimate the constraints for galaxy mass and size to allow the MBH merger. In Fig. 3, we show the mass and size of galaxies in which MBHs successively merge during  $140t_{\text{dy,g}}$ . They have the stellar velocity dispersion of more than  $180 \text{ km s}^{-1}$ . Using Equation (3), we relate their masses to their sizes as

$$\left( \frac{M_g}{10^{10}M_\odot} \right) \gtrsim 1.5 \left( \frac{r_g}{1\text{kpc}} \right). \quad (14)$$

Such regions are above the solid lines in the top panels of Fig. 3.

We also impose the conditions on which the successive mergers of MBHs occurs within 1 Gyr or within 10 Gyr. If the merger timescale is  $140t_{\text{dy,g}}$ , the galaxies should have their dynamical time of less than 7 Myr for 1 Gyr case or 70 Myr for 10 Gyr case. Using Equation (3) and (4), we obtain

$$\left( \frac{M_g}{10^9M_\odot} \right) = 1.1 \left( \frac{t_{\text{dy,g}}}{14\text{Myr}} \right)^{-2} \left( \frac{r_g}{1\text{kpc}} \right)^3. \quad (15)$$

Therefore, we can write the relation between their masses and sizes:

$$\left( \frac{M_g}{10^9M_\odot} \right) > \begin{cases} 4.4 \left( \frac{r_g}{1\text{kpc}} \right)^3 & \cdots 1 \text{ Gyr case} \\ 0.044 \left( \frac{r_g}{1\text{kpc}} \right)^3 & \cdots 10 \text{ Gyr case} \end{cases} \quad (16)$$

These regions are upper sides of the dashed lines in the top panels of Fig. 3. As a result, the shaded regions in the top panels of Fig. 3 are the allowed regions for the masses and sizes of galaxies in which MBHs can successively merge.

These constraints can be translated into those for the mass ( $M_h$ ) and size ( $r_h$ ) of a dark matter halo, using a simplified model. A dark matter halo is assumed to be six times

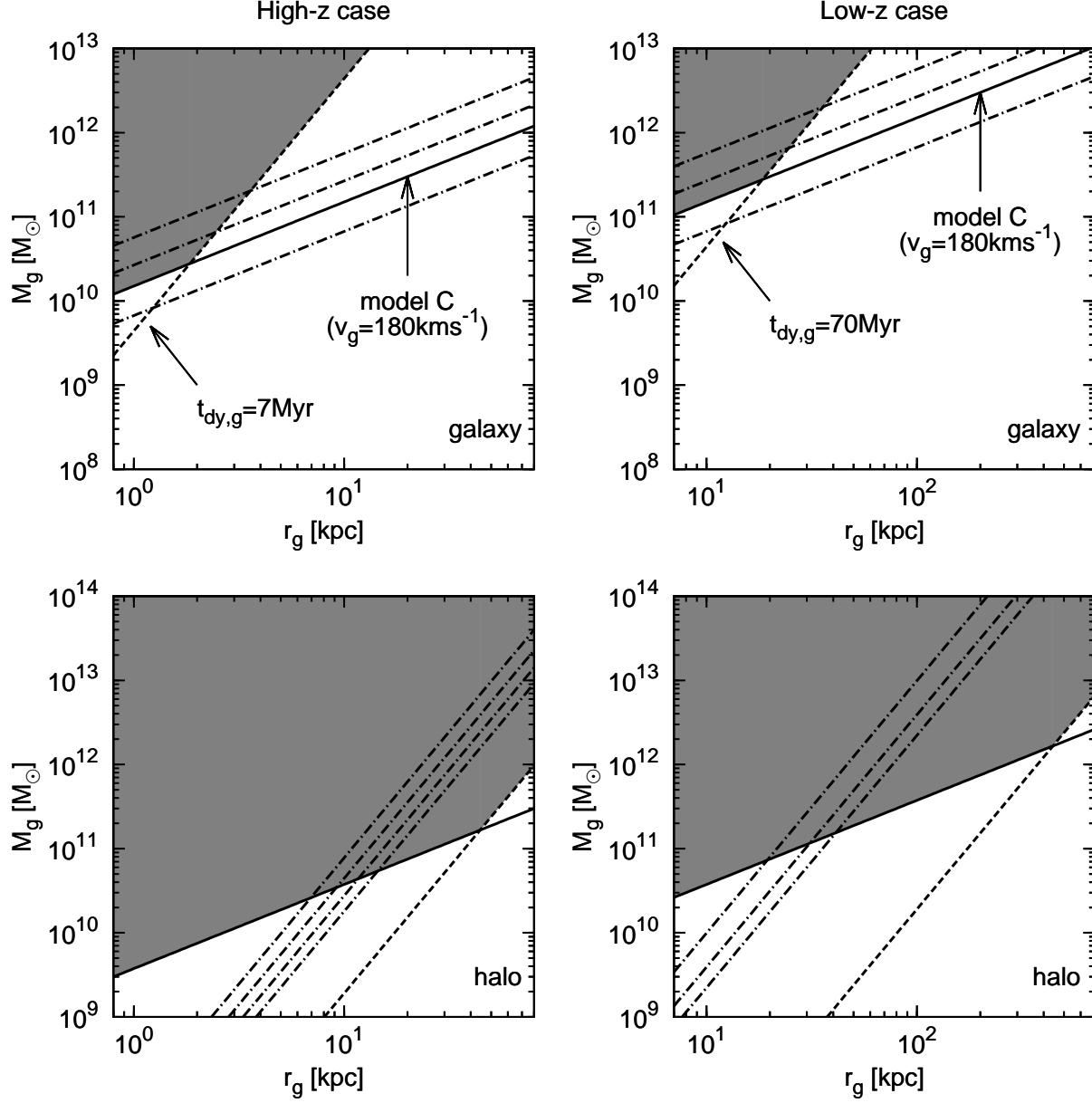


**Figure 3.** Mass and size of a galaxy (top panels) and halo containing the galaxy (bottom panels). In left and right panels, gray regions indicate the galaxy and halo in which MBHs merge within 1 Gyr and 10 Gyr, respectively. In the top panels, the solid lines correspond to a galaxy of model C, and the dashed lines indicate galaxies with  $t_{\text{dy,g}} = 7 \text{ Myr}$  (left) and 70 Myr (right). The dashed-dotted lines in the top left and right panels correspond to galaxies of models A, B, and D from top to bottom. In the bottom panels, the dashed-dotted lines show mass and size of a halo formed at redshift  $z = 15, 10, 7$ , and 5 (from left to right) in the left panel, and those of a halo formed at redshift  $z = 3, 1$ , and 0 (from left to right) in the right panel.

more massive than that of a galactic stellar component, according to the ratio of dark matter to baryon in the universe (Komatsu et al. 2011). However, stellar components are more concentrated than the dark matter components due to cooling when stars are formed. Hence, the dark matter halo does not seem to make a significant effect on the merger dynamics. Actually, dark matter mass at the central region is much less than or at most comparable to stellar mass (e.g. Forman, Jones & Tucker 1985; Saglia & Bertin 1992). In the present analysis, the stellar velocity dispersion is assumed to be twice of the velocity dispersion in the dark matter halo.

This is justified by the difference between observed velocity dispersions at effective radii and those at several effective radii in elliptical galaxies (Coccato et al. 2009). Then, the size of the dark matter halo is 24 times larger than that of the stellar component from virial theorem. Using these relations, we can obtain the regions of the masses and sizes of dark matter haloes in which MBHs successively merge, which are the shaded regions in the bottom panels of Fig. 3.

The formation epoch (redshift) can be assessed depending on the masses and sizes of dark matter haloes, in the same way as Mo, Mao & White (1998). We equate the size

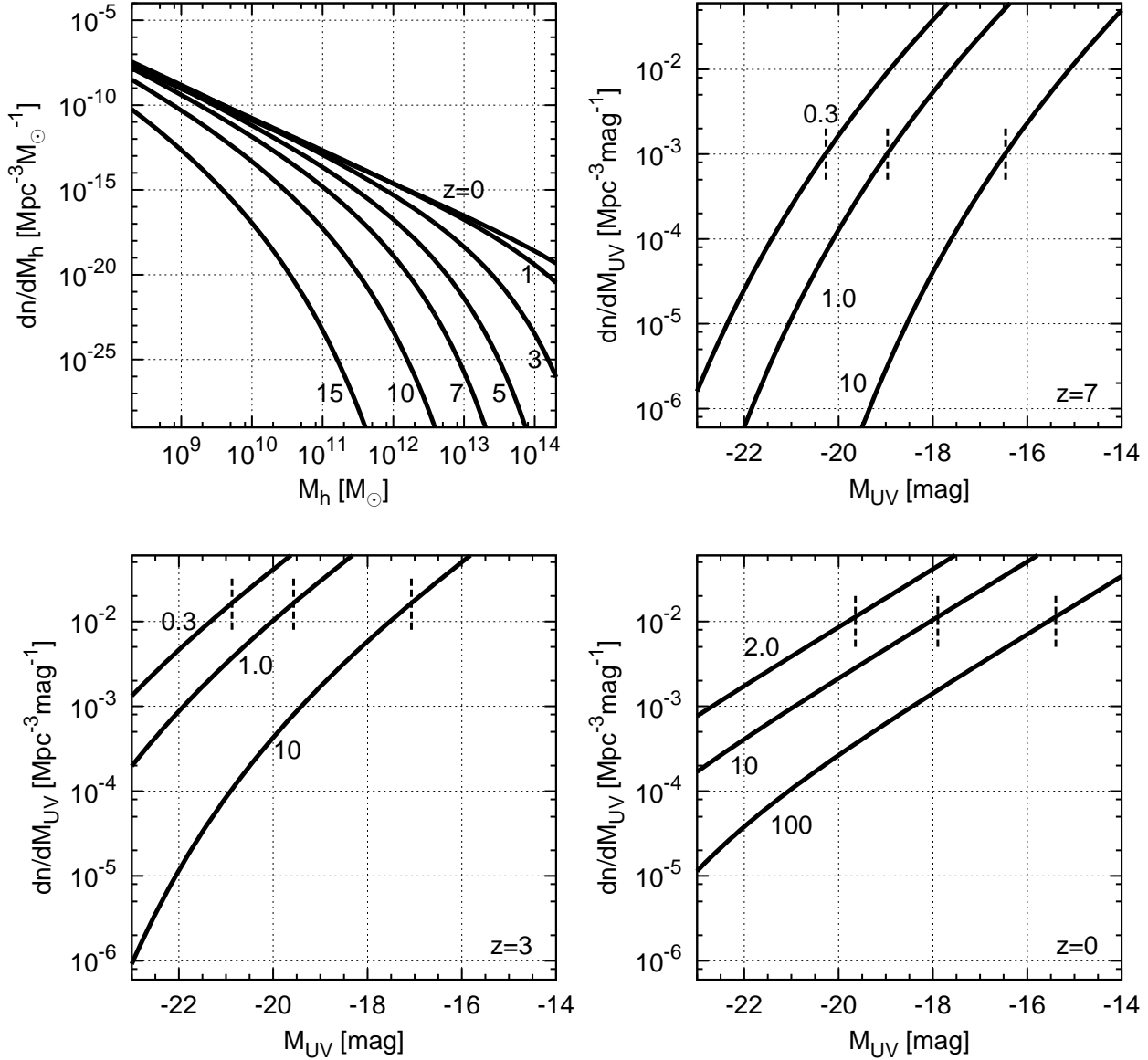


**Figure 4.** (Top left) Press-Schechter mass function at a given redshift. Cosmological constants are set as  $(\Omega_\Lambda, \Omega_m, h, k, \sigma_8) = (0.7, 0.3, 0.7, 1, 0.8)$ . (Others) UV luminosity functions of galaxies at redshift  $z = 7, 3$ , and  $0$ . In more luminous galaxies that the luminosity indicated by vertical dashed lines on each curve, MBHs successively merge. The number beside each curve shows assumed mass-to-light ratio to obtain each UV luminosity function.

of a dark matter halo ( $r_h$ ) to the radius inside which the mean mass density is 200 times the critical density at a given redshift  $z$ , and then derive the mass of a dark matter halo ( $M_h$ ) inside  $r_h$ . The virial mass and radius are related as

$$M_h = 100 G^{-1} H(z)^2 r_h^3. \quad (17)$$

We can rewrite Equation (17) as

$$\left( \frac{M_h}{10^{11} M_\odot} \right) = 12 \left[ \frac{H(z)}{H(10)} \right]^2 \left( \frac{r_h}{30 \text{ kpc}} \right)^3. \quad (18)$$

The function  $H(z)$  is expressed as

$$H(z) = H_0 [\Omega_\Lambda + (1 - \Omega_\Lambda - \Omega_m)(1+z)^2 + \Omega_m(1+z)^3]^{1/2}, \quad (19)$$

where  $H_0$  is the Hubble constant, and  $\Omega_\Lambda$  and  $\Omega_m$  are the lambda parameter and the matter density parameter, respectively. In Equation (18), we adopt  $(\Omega_\Lambda, \Omega_m) = (0.7, 0.3)$ , and hereafter we also adopt these values and  $h = 0.7$ , where the Hubble constant is  $H_0 = 100h \text{ km s}^{-1} \text{ Mpc}^{-1}$ . From these equations, we can draw the relation between masses and sizes of dark matter haloes at formation redshifts, which is shown by dashed-dotted lines in the bottom panels of Fig. 3.

From the bottom panels of Fig. 3, we can estimate the minimum mass of a dark matter halo which allows MBH successive mergers at a given redshift. In order for the merger to occur during 1 Gyr, dark matter haloes formed at redshift

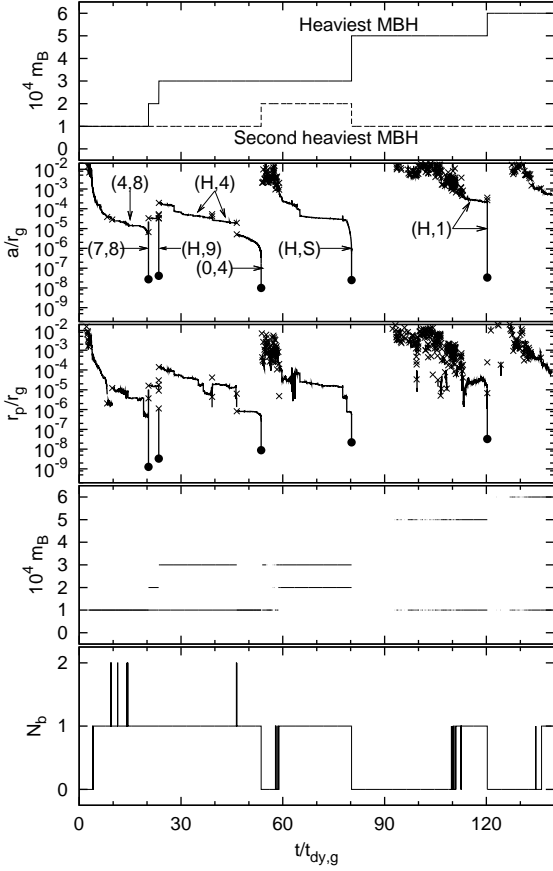


**Figure 2.** Time evolution of MBHs in model A1. The top panel shows the masses of the heaviest and second heaviest MBHs at each time. We indicate parameters of the binary MBH with the smallest semi-major axis at each time, i.e. its semi-major axis (second top), the distance at the pericentre (middle), and component masses (second bottom). The bottom panel shows the number of binary MBHs whose semi-major axes are less than  $10^{-3}r_g$ . Pairs of integers in parentheses in the second top panel show the labels of MBHs composing the binary MBHs, where the heaviest MBH is labelled with “H” and the second heaviest one is “S”. We attached labels only to binary MBHs which are long-lived, or merge eventually. In the second top and middle panels, filled circles indicate the moments when MBHs merge and crosses denote those when binary components are exchanged.

$z = 7$  should have more than  $4 \times 10^{10} M_\odot$ , which corresponds to the stellar component mass of about  $6.7 \times 10^9 M_\odot$ . In the case of mergers during 10 Gyr, dark matter haloes formed at redshift  $z = 3$  should have more than  $7 \times 10^{10} M_\odot$ .

If there were only one binary MBH in a nonaxisymmetric galactic potential, the timescale for the merger is about 10 Gyr or 0.3 Gyr respectively for the stellar component of  $10^9 M_\odot$  or  $10^{11} M_\odot$  (Khan, Just & Merritt 2011). Therefore, at redshifts of  $z \gtrsim 7$ , when the cosmic age is less than 1 Gyr, another MBH may intrude before a binary MBH merges. Our results show that even if multiple MBHs exist in a galaxy with  $4 \times 10^{10} M_\odot$  at redshift  $z = 7$ , the MBHs can successively merge.

## 4.2 Merger criteria for galactic luminosity

In the above, we have derived the constraints for the masses and sizes of galaxies and their parent dark haloes, in which the successive merger of MBHs can occur. Here, we compare the luminosity function based on the Press-Schechter formalism. The luminosity function of galaxies is obtained as follows. We can give an ultraviolet (UV) magnitude of a galaxy embedded in a halo with mass  $M_h$  as

$$M_{UV} = M_{UV,\odot} - \frac{2.5}{\log 10} \log \left[ \left( \frac{M_h}{M_\odot} \right) \left( \frac{\Omega_b}{\Omega_m} \right) \Upsilon_{UV,\odot}^{-1} \right], \quad (20)$$

where  $M_{UV,\odot}$  is UV magnitude of the Sun,  $\Upsilon_{UV,\odot}$  is the mass-to-UV luminosity ratios scaled by that of the Sun. We set  $M_{UV,\odot} = 5.6$ . Here, we assume that a galaxy mass  $M_g$  is equal to  $(\Omega_m/\Omega_b)^{-1} M_h$ , and that  $\Omega_m/\Omega_b = 6$ . We denote the number density of haloes by  $n$ . Note that  $n$  can be regarded as the number density of galaxies, since we assume a halo has one galaxy. Then, Press-Schechter mass function of dark matter haloes (shown in the top left panel of Fig. 4) can be transformed into the luminosity function at UV band as

$$\frac{dn}{dM_{UV}} = - \frac{d(M_h/M_\odot)}{dM_{UV}} \frac{dn}{d(M_h/M_\odot)} \quad (21)$$

$$= \frac{\log 10}{2.5} \left( \frac{M_h}{M_\odot} \right) \frac{dn}{d(M_h/M_\odot)}. \quad (22)$$

Observationally, the mass-to-luminosity ratios for high-redshift Ly  $\alpha$  emitters (LAEs),  $\Upsilon_{UV,\odot}$ , can range from 0.3 to 10 (Fernandez & Komatsu 2008). For low-redshift galaxies, the mass-to-luminosity ratios range from 2 to 10 in normal galaxies, but reach  $\sim 100$  in dwarf galaxies (Hirashita, Takeuchi & Tamura 1998; Strigari et al. 2008). Considering the observed mass-to-luminosity ratios, we draw the UV luminosity function  $dn/d(M_{UV}/M_\odot)$  in Fig. 4 for the cases of redshift  $z = 7$  (top right), 3 (bottom left), and 0 (bottom right). In each panel, we show the UV luminosity function  $dn/d(M_{UV}/M_\odot)$  with different  $\Upsilon_{UV,\odot}$ . The values of  $\Upsilon_{UV,\odot}$  are indicated by numbers beside the curves. The critical luminosity of galaxies for the successive mergers is shown by vertical dashed lines attached with each curve. The successive mergers happen in galaxies brighter than the critical luminosities.

Observed luminosity functions of high-redshift LAEs (Ouchi et al. 2009) and those of Lyman break galaxies (LBGs) (Jiang et al. 2011) seem to match well the curves with  $\Upsilon_{UV,\odot} \sim 1$ . Thus, the successive MBH merger is expected for LAEs or LBGs brighter than  $M_{UV} \simeq -19$  (see the top right and bottom left panels of Fig. 4). Since  $\Upsilon_{UV,\odot} = 2 - 10$  in low-redshift galaxies, the successive merger is expected for low-redshift galaxies brighter than  $M_{UV} \simeq -18$  (see the bottom right panel of Fig. 4). Note that if  $\Upsilon_{UV,\odot}$  is as large as 100 in dwarf galaxies, the critical UV magnitude can be overestimated by about a factor of two. These dwarf galaxies would lose an amount of baryons through their evolution. Although we adopt  $\Omega_m/\Omega_b = 6$  for all galaxies,  $\Omega_m/\Omega_b$  should be set to a larger value for these dwarf galaxies. If we do so, the curve of  $\Upsilon_{UV,\odot} = 100$  in the bottom right panel of Fig. 4 will shift leftward.



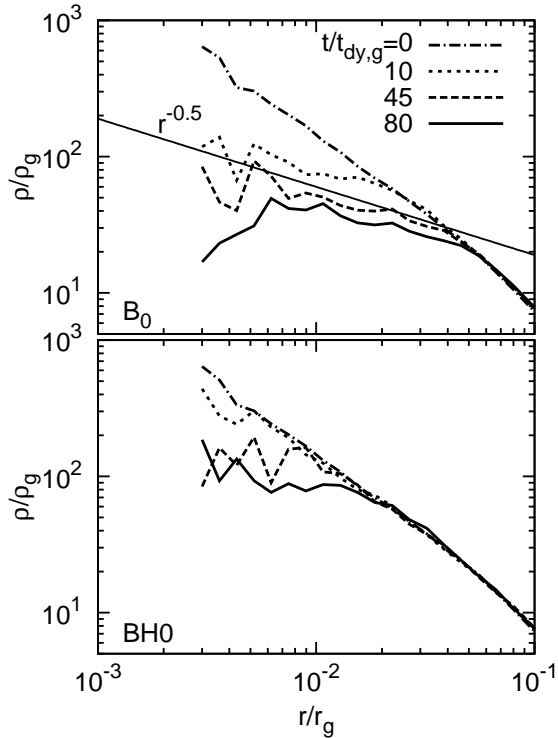


**Figure 5.** Mass density profile of stars in a galaxy with ten MBHs (top) or without MBHs (bottom). In both panels, dashed-dotted, dotted, dashed, and solid curves indicate the mass density at  $t/t_{\text{dy,g}} = 0, 10, 45$ , and  $80$ , respectively. A solid line in the top panel shows the relation of  $\rho \propto r^{-0.5}$ .

## 5 BACK-REACTION TO A HOST GALAXY

### 5.1 Galaxy structure

Hereafter, we focus on the simulation results of model B<sub>0</sub>. If necessary, we can compare a simulation including the GW recoil, model B<sub>1</sub>. Fig. 5 shows the evolution of mass density profile of stars (the top panel). The mass density inside  $r/r_g = 0.05$  decreases gradually. This is because MBHs give their kinetic energy to stars as a back reaction of dynamical friction and sling-shot mechanism. Until  $t/t_{\text{dy,g}} = 80$ , six MBHs merge. We can see in the top panel of Fig. 5 that the mass density profile is roughly proportional to  $r^{-0.5}$  in the range from  $r/r_g = 5 \times 10^{-3}$  to  $r/r_g = 0.05$ . Such a density slope is consistent with those in a galaxy with two MBHs and three MBHs (Nakano & Makino 1999; Iwasawa, Funato & Makino 2008). In Fig. 6, we see an enclosed mass of the galaxy within  $r/r_g = 0.05$  (vertical dashed line) is  $10^{-2} M_g$ , which is ten times higher than the total mass of MBHs. Hence, the present simulation shows that MBHs can affect the galactic structure of the central regions that include about ten times the total mass of MBHs.

We also compare the structure of the galaxy containing ten MBHs to that containing two MBHs. The total masses of MBHs are the same, that is, 0.1 % of the galaxy mass in both of the models. The top panel of Fig. 7 shows the mass density profile of the galaxy with ten MBHs at  $t/t_{\text{dy,g}} = 79, 80$  and  $81$ . The mass density is not fluctuated on the dynamical timescale in the range from  $r/r_g = 0.01$  to  $0.05$ .

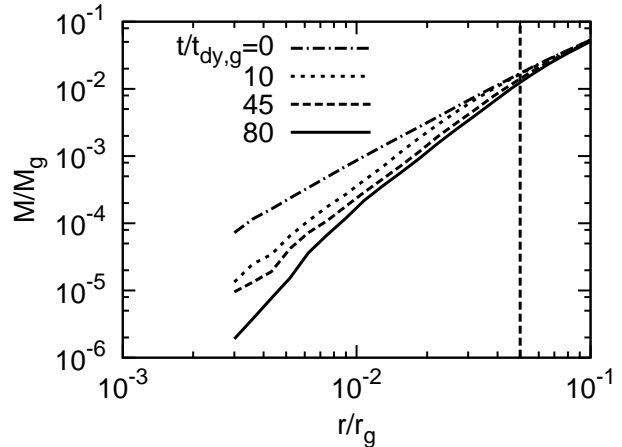


**Figure 6.** Mass of stars within each radius in model B<sub>0</sub> with ten MBHs. Dashed-dotted, dotted, dashed, and solid curves indicate the mass at the time  $t/t_{\text{dy,g}} = 0, 10, 45$ , and  $80$ . The vertical dashed line indicates  $r/r_g = 0.05$ .

In the middle panel of Fig. 7, we show the mass density profile of the galaxy with two MBHs at  $t/t_{\text{dy,g}} = 30, 40$ , and  $50$ . During 20 dynamical time, the mass density profile is not changed in the case of the galaxy with two MBHs. We expect that the mass density profile is never changed after  $t/t_{\text{dy,g}} = 50$ .

In the bottom panel of Fig. 7, we compare the mass density profile of the galaxy containing ten MBHs at  $t/t_{\text{dy,g}} = 80$  with those containing two MBHs at  $t/t_{\text{dy,g}} = 50$ . Both of the mass density slopes are proportional to  $r^{-0.5}$ . However, the mass density of the galaxy with ten MBHs is lower by a factor of 1.5 than that with two MBHs. This difference results from the sling-shot mechanism in the galaxy with ten MBHs. Owing to the sling-shot mechanism among three MBHs, MBHs receive kinetic energy, and transfer their kinetic energy to stars through the dynamical friction. Such picture is consistent with a galaxy with three MBHs (Iwasawa, Funato & Makino 2008).

Here, we verify that the central density of a galaxy in model B<sub>0</sub> are decreased by MBH dynamics, not by artificial two-body relaxation. The bottom panel of Fig. 5 shows the evolution of mass density profile of a galaxy without any MBH, in which only two-body relaxation decreases the central mass density of the galaxy. Comparing mass densities in the top and bottom panels of Fig. 5, we can see that the central density in model B<sub>0</sub> is decreased much more rapidly than that in model BH0. Therefore, the central density of a galaxy in model B<sub>0</sub> are dominantly decreased by MBH dynamics.

### 5.2 High-velocity stars

We investigate stars which are ejected from a galaxy with high speed. Such stars are generated through the sling-shot mechanism induced by a binary MBH. We focus on the simulation results of model B<sub>0</sub>. If necessary, we can compare a simulation including the GW recoil, model B<sub>1</sub>, in which MBHs also successively merge.

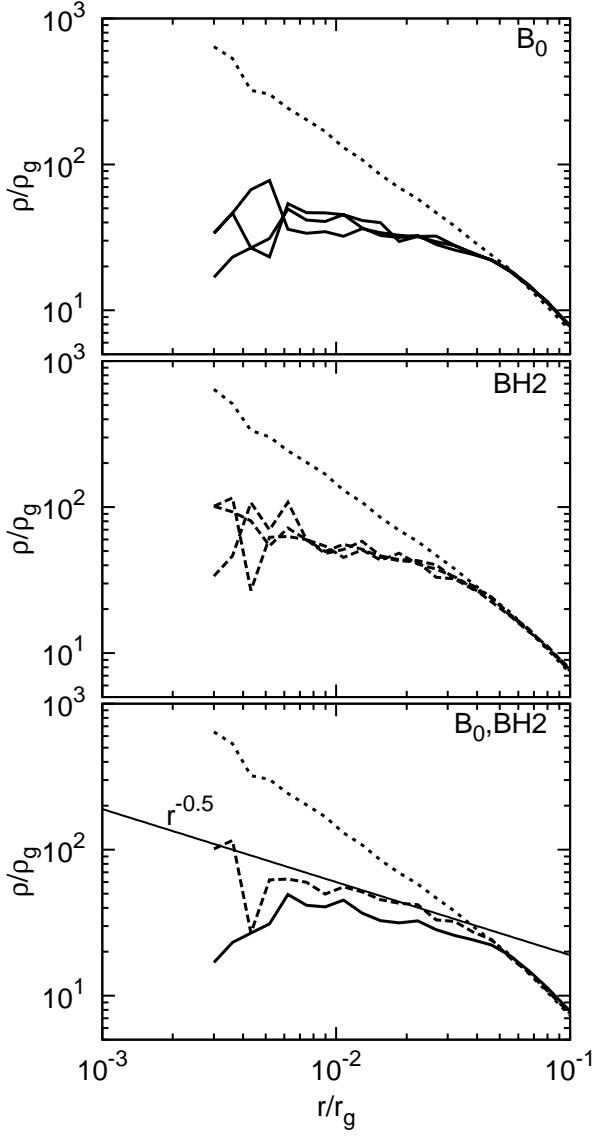


**Figure 7.** Mass density profile of a galaxy with ten MBHs (top), that with two MBHs (middle), and both (bottom). In all the panels, the dotted curve shows the profile at the initial time. In the top panel, the solid curves indicate the profile at the time  $t/t_{\text{dy,g}} = 79, 80$ , and  $81$ . In the middle panel, the dashed curves indicate the profile at the time  $t/t_{\text{dy,g}} = 30, 40$ , and  $50$ . In the bottom panel, the solid and dashed curves are the profiles of a galaxy with ten MBHs at  $t/t_{\text{dy,g}} = 80$ , and a galaxy with two MBHs at  $t/t_{\text{dy,g}} = 50$ , respectively.

We compare the velocity distributions of stars as a function of  $\theta$  at the time  $t/t_{\text{dy,g}} = 0$  and  $80$  in the cases of models with and without MBHs. We illustrate the relation of  $\theta$  to the position and velocity vectors in Fig. 8. Then, the  $\theta$  is expressed as

$$\theta = \cos^{-1} \left( \frac{\mathbf{r}_f \cdot \mathbf{v}_f}{r_f v_f} \right), \quad (23)$$

where  $\mathbf{r}_f$  and  $\mathbf{v}_f$  are respectively the position and velocity vectors of a star, and  $r_f = |\mathbf{r}_f|$  and  $v_f = |\mathbf{v}_f|$ . The origin of the position vector is set to the galaxy centre.

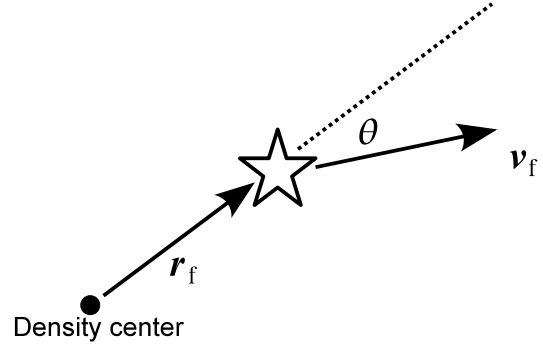


**Figure 8.** Illustration of the position vector ( $\mathbf{r}_f$ ), velocity vector ( $\mathbf{v}_f$ ) of a star, and  $\theta$ .

We define high-velocity stars as stars whose velocities are more than  $2\sqrt{2}v_g$ . Fig. 9 shows the resultant velocity distributions of stars. The presence of high-velocity stars is an outstanding feature of model  $B_0$  at the time  $t_{\text{dy,g}} = 80$  (the second top panel). We also find such high-velocity stars in a galaxy with two MBHs, model BH2 (the second bottom panel). We can see that some stars have velocities higher than  $v_f/v_g = 10$ . Furthermore, they have extremely radial orbits around  $\theta = 0$ . This is because they are generated at the galactic centre through the sling-shot mechanism by a binary MBH, and directly go away outside the galaxy. Note that no high-velocity star is generated in a galaxy without MBHs, model BH0 (see the bottom panel of Fig. 9).

We investigate the difference between properties of high-velocity stars in the cases of galaxies with ten MBHs and with two MBHs. 37 high-velocity stars have been generated at  $t/t_{\text{dy,g}} = 80$  in model  $B_0$ , in contrast to 188 high-velocity stars at  $t/t_{\text{dy,g}} = 50$  in model BH2. The generation rate of high-velocity stars in model  $B_0$  is ten times lower than that in model BH2. This is because a galaxy with ten MBHs does not always have a binary MBH with small semi-major axis, while a binary MBH stays in the central region of the galaxy in model BH2 (see the top panel of Fig. 10). It is difficult for a binary MBH to produce high-velocity stars, unless its semi-major axis is as small as  $\sim 10^{-5}r_g$ . This is readily estimated with numerical results by Quinlan (1996). A binary MBH typically gives a kick velocity of the order of  $v_{\text{kick}} = \sqrt{2.5G\mu/a}$  to a field star through the sling-shot mechanism, where  $\mu$  and  $a$  are the reduced mass and semi-major axis of a binary MBH. Supposing that a binary MBH consists of two MBHs with the initial mass, a binary with the semi-major axis of  $a < 3.3 \times 10^{-5}r_g$  can produce high-velocity stars with  $v_{\text{kick}} > 2\sqrt{2}v_g$ .

Another possible reason is that more stars interact with a binary MBH in model BH2, since the total mass of the binary MBH in model BH2 is larger than that in model  $B_0$ .

The total number of high-velocity stars increases in different ways between models  $B_0$  and BH2. As seen in the bottom panel of Fig. 10, the number of high-velocity stars increases at a roughly constant rate in model BH2 from the time  $t/t_{\text{dy,g}} = 10$  to  $50$ . On the other hand, the generation rate of high-velocity stars is largely changed in model  $B_0$  from the time  $t/t_{\text{dy,g}} = 0$  to  $80$  (see the solid curve in the bottom panel of Fig. 10). The generation rate is low during the time  $t/t_{\text{dy,g}} = 40 - 60$ , and during  $t/t_{\text{dy,g}} = 70 -$

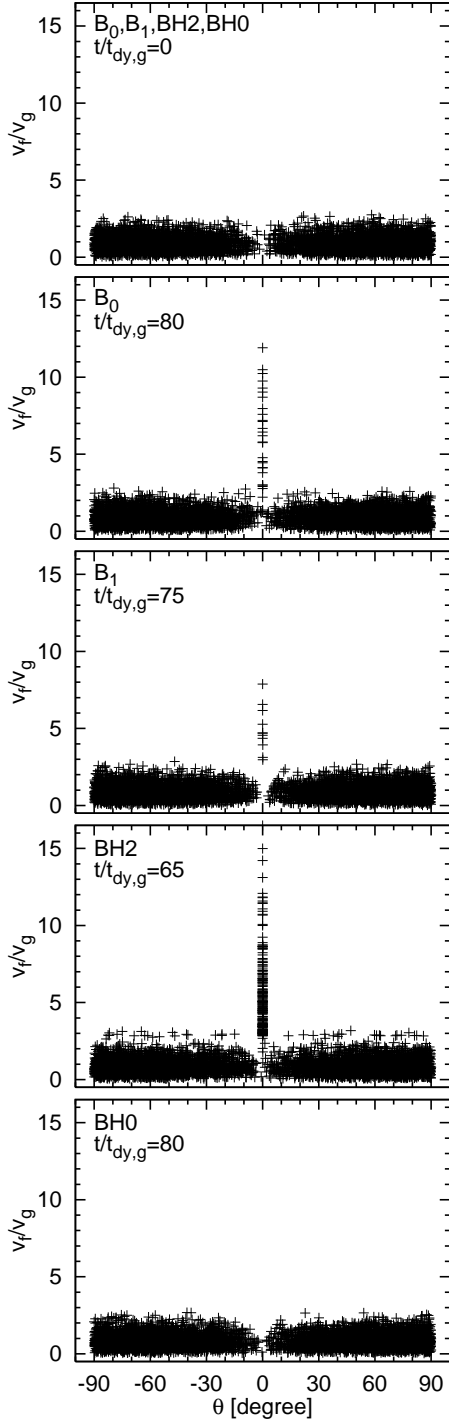


**Figure 9.** Velocity distributions of stars as a function of  $\theta$  in models  $B_0$ ,  $B_1$ ,  $BH2$ , and  $BH0$  at the initial time (top), in model  $B_0$  at  $t/t_{dy,g} = 80$  (second top), in model  $B_1$  at  $t/t_{dy,g} = 75$  (middle), in model  $BH2$  at  $t/t_{dy,g} = 65$  (second bottom), and in model  $BH0$  at  $t/t_{dy,g} = 80$  (bottom).

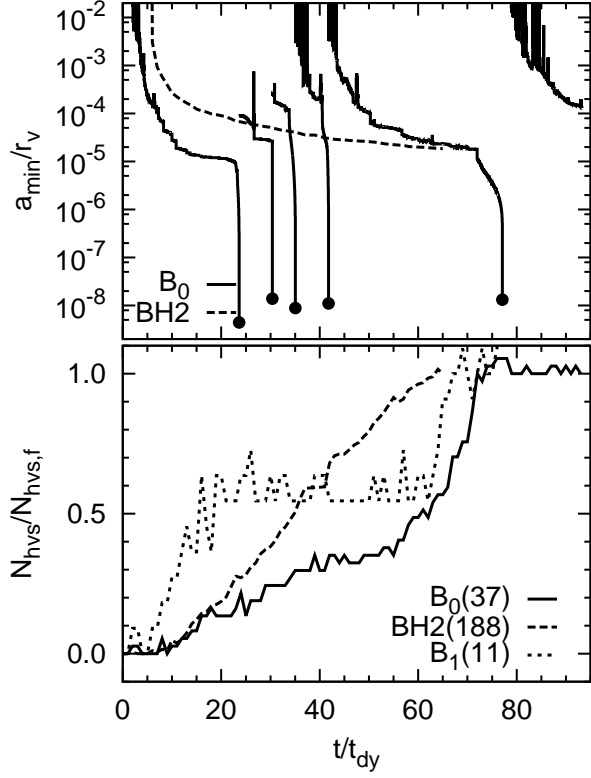


**Figure 10.** Time evolution of the minimum semi-major axis of a binary MBH at each time (top), and the number of high-velocity stars scaled by its final number (bottom). High-velocity stars are defined as those whose velocities are more than  $2\sqrt{2}v_g$ .

90, while it is high during  $t/t_{dy,g} = 10 - 40$  and during  $t/t_{dy,g} = 60 - 70$ . This feature is similar to high-velocity stars in model  $B_1$ .

In a galaxy with ten MBHs, such as models  $B_0$  and  $B_1$ , high-velocity stars are generated intermittently because of the occasional absence of a binary MBH whose semi-major axis is favourable to eject stars,  $\sim 10^{-5}r_g$ . This can be verified in models  $B_0$  and  $BH2$ . During  $t_{dy,g} = 10 - 40$ , and  $60 - 70$ , high-velocity stars are generated at a high rate in model  $B_0$  (see the bottom panel of Fig. 10). At this time, there is a binary MBH with semi-major axis of about  $10^{-5}r_g$  (see the top panel of Fig. 10). The generation rate of high-velocity stars is low during  $t_{dy,g} = 10 - 20$ ,  $40 - 60$ , and  $70 - 90$ . Except  $t_{dy,g} = 70 - 80$ , there is a binary MBH with semi-major axis much larger than  $10^{-5}r_g$ , or no binary MBH. Therefore, stars are not ejected through sling-shot mechanism. During  $t_{dy,g} = 70 - 80$ , there is a binary MBH with semi-major axis much less than  $10^{-5}r_g$ . Such a binary MBH cannot interact with stars due to small cross section. On the other hand, there is a binary MBH with semi-major axis  $\sim 10^{-5}r_g$  in model  $BH2$ .

The feature of the intermittent generation rate can be a useful probe to constrain the formation mechanism of a single merged MBH, or a binary MBH at the galaxy centre at the present time.

## 6 SUMMARY

We have performed  $N$ -body simulations to investigate successive mergers of MBHs in galaxies with different masses and radii. We have found that about a half of multiple MBHs successively merge to one bigger MBH within  $140t_{\text{dy,g}}$  in galaxies with the velocity dispersion larger than  $\sim 180 \text{ km s}^{-1}$ . The merger of MBHs is promoted, such that the loss cone of binary MBHs is refilled by MBHs losing their angular momenta due to dynamical friction. GW recoil does not affect the merger process, if the recoil velocity is of the order of the stellar velocity dispersion. Galaxies which allow multiple MBHs to merge should reside in dark matter haloes with the mass more than  $4 \times 10^{10} M_{\odot}$ , if these dark matter haloes form at high redshifts. These galaxies could correspond to LAEs or LBGs brighter than the UV magnitude  $M_{\text{UV}} \simeq -19$  at high redshifts. On the other hand, an MBH which has experienced the successive merger can inhabit low-redshift galaxies brighter than  $M_{\text{UV}} \simeq -18$ .

We have also investigated the evolution of the galactic structure and the generation of high-velocity stars as the back-reaction by the successive merger of MBHs. We have found that the dynamics of MBHs affects the central regions of galaxy that contain about ten times the total mass of MBHs. The mass density profile is transformed to  $\rho \propto r^{-0.5}$ , which is the same as the mass density profile in the case of a galaxy with two and three MBHs. The mass density in the central regions is 1.5 times smaller than in the case of the galaxy with two MBHs. In a galaxy with ten MBHs, high-velocity stars are generated intermittently, while they are generated at a constant rate in the case of a galaxy with two MBHs. Such features should enable us to constrain the merger mechanism of MBHs in a galaxy.

## ACKNOWLEDGEMENTS

We thank Kohji Yoshikawa for fruitful advice on cosmological arguments, Masaki Iwasawa for useful comments about our simulation method, and Yuichi Matsuda for stimulating discussion. Numerical simulations have been performed with computational facilities at the Center for Computational Sciences in the University of Tsukuba. This work was supported in part by the FIRST project based on the Grants-in-Aid for Specially Promoted Research by MEXT (16002003), and Grant-in-Aid for Scientific Research (S) by JSPS (20224002).

## REFERENCES

- Abel T., Bryan G. L., Norman M. L., 2000, *ApJ*, 540, 39  
 Abramowicz M. A., Czerny B., Lasota J. P., Szuszkiewicz E., 1988, *ApJ*, 332, 646  
 Begelman M. C., Blandford R. D., Rees M. J., 1980, *Nature*, 287, 307  
 Berczik P., Merritt D., Spurzem R., Bischof H., 2006, *ApJ*, 642, 21  
 Berentzen I., Preto M., Berczik P., Merritt D., Spurzem R., 2009, *ApJ*, 695, 455  
 Blaes O., Lee M. H., Socrates A., 2002, *ApJ*, 578, 775  
 Bromm V., Coppi P. S., Larson R. B., 2002, *ApJ*, 564, 23  
 Burkert A., Tremaine S., 2010, *ApJ*, 720, 516  
 Campanelli M., Lousto C., Zlochower Y., Merritt D., 2007, *ApJ*, 659, 5  
 Casertano S., Hut P., 1985, *ApJ*, 298, 80  
 Clark P. C., Glover S. C. O., Klessen R. S., Bromm V., 2011, *ApJ*, 727, 110  
 Coccato L. et al., 2009, *MNRAS*, 394, 1249  
 Damour T., Dervelle N., 1981, *Physics letters A*, 87, 81  
 Djorgovski S. G., Courbin F., Meylan G., Sluse D., Thompson D., Mahabal A., Glikman E., 2007, *ApJ*, 662, L1  
 Fabrycky D., Tremaine S., 2007, *ApJ*, 669, 1298  
 Fan X. et al., 2001, *AJ*, 122, 2833  
 Farina E. P., Montuori C., Decarli R., Fumagalli M., 2013, *MNRAS*, 431, 1019  
 Fernandez E. R., Komatsu E., 2008, *MNRAS*, 384, 1363  
 Ferrarese L., Merritt D., 2000, *ApJ*, 539, L9  
 Forman W., Jones C., Tucker W., 1985, *ApJ*, 293, 102  
 Fukushige T., Makino J., Kawai A., 2005, *PASJ*, 57, 1009  
 Greene J. E., 2012, *Nature Communications*, 3, 1304  
 Gültekin K., Richstone D. O. et al., 2009, *ApJ*, 698, 198  
 Harris G. L. H., Harris W. E., 2011, *MNRAS*, 410, 2347  
 Hirashita H., Takeuchi T. T., Tamura, N., 1998, *ApJ*, 504, L83  
 Hosokawa T., Omukai K., Yoshida N., Yorke H., 2011, *Science*, 334, 1250  
 Iwasawa M., Funato Y., Makino J., 2006, *ApJ*, 651, 1059  
 Iwasawa M., Funato Y., Makino J., 2008, preprint (arXiv:0801.0859)  
 Iwasawa M., An S., Matsubayashi T., Funato Y., Makino J., 2011, *ApJ*, 731, L9  
 Jiang L. et al., 2011, *ApJ*, 743, 65  
 Kawaguchi T., 2003, *ApJ*, 593, 69  
 Kesden M., Sperhake U., Berti E., 2010, *ApJ*, 715, 1006  
 Khan F. M., Just A., Merritt D., 2011, *ApJ*, 732, 89  
 Khan F. M., Preto M., Berczik P., Berentzen I., Just A., Spurzem R., 2012, *ApJ*, 749, 147  
 Komatsu E. et al., 2011, *ApJS*, 192, 18  
 Kormendy J., Richstone D., 1995, *ARA&A*, 33, 581  
 Kozai Y., 1962, *AJ*, 67, 591  
 Kupi G., Amaro-Seoane P., Spurzem R., 2006, *MNRAS*, 371, 45  
 Liu X., Shen Y., Strauss M. A., 2011, *ApJ*, 736, L7  
 Lousto C. O., Campanelli M., Yosef Z., Nakano H., 2010, *Classical and Quantum Gravity*, 27, 114006  
 Makino J., Aarseth S., 1992, *PASJ*, 44, 141  
 Makino J., Fukushige T., Koga M., Namura K., 2003, *PASJ*, 55, 1163  
 Magorrian J. et al. 1998, *ApJ*, 115, 2285  
 Marconi A., Hunt L. K., 2003, *ApJ*, 589, L21  
 Marconi A. et al., 2004, *MNRAS*, 351, 169  
 Matsui H. et al., 2012, *ApJ*, 746, 26  
 Merritt D., Poon M. Y., 2004, *ApJ*, 606, 788  
 Miller M. C., Hamilton D. P., 2002, *ApJ*, 576, 894  
 Milosavljevic M., Couch S. M., Bromm V., 2009, *ApJ*, 696, 146 (Milosavljevic et al. 2009a)  
 Milosavljevic M., Bromm V., Couch S. M., Oh S. P., 2009, *ApJ*, 698, 766 (Milosavljevic et al. 2009b)  
 Mo H. J., Mao S., White S. D. M., 1998, *MNRAS*, 295, 319  
 Nakamura F., Umemura M., 2001, *ApJ*, 548, 19  
 Nakano T., Makino J., 1999, *ApJ*, 510, 155  
 Ohsuga K., Mori M., Nakamoto T., Mineshige S., 2005, *ApJ*, 628, 368  
 Ouchi M. et al., 2009, *ApJ*, 706, 1136

- Quinlan G. D., 1996, *NewA*, 1, 35  
Saglia R. P., Bertin G., 1992, *ApJ*, 384, 433  
Schawinski K., Urry M., Treister E., Simmons B., Natarajan P., Glikman E., 2011, *ApJ*, 743, L37  
Soffel M. H., 1989, *Relativity in Astrometry, Celestial Mechanics and Geodesy*. Berlin Springer  
Soltan A., 1982, *MNRAS*, 200, 1155  
Strigari L. E. et al., 2008, *Nature*, 454, 1096  
Sugimoto D., Chikada Y., Makino J., Ito T., Ebisuzaki T., Umemura M., 1990, *Nature*, 345, 33  
Tanikawa A., Umemura M., 2011, *ApJ*, 728, L31 (paper I)  
Tremaine S. et al. 2002, *ApJ*, 574, 740  
Umemura M., 2001, *ApJ*, 560, L29  
Umemura M., Susa H., Suwa T., Sato D., eds. *Proc. AIP. Conf. 990, First Stars III*, Melville, NY:AIP, p. 386  
Yoshida N., Omukai K., Hernquist L., Abel T., 2006, *ApJ*, 652, 6  
Yu Q., Tremaine S. 2002, *MNRAS*, 335, 965

This paper has been typeset from a  $\text{\LaTeX}$  file prepared by the author.